KERNFORSCHUNGSZENTRUM KARLSRUHE

Februar 1966

KFK 403

Institut für Experimentelle Kernphysik

Studies on Crossbar and Slotted Iris Structures for a Proton-Linear-Accelerator

W. Bauer, H. Eschelbacher, M. Kuntze

GESELLSCHAFT FUR KERNFORSCHUNG M. B. H.

KARLSRUHE

KERNFORSCHUNGSZENTRUM KARLSRUHE

Februar 1966 KFK 403

Institut für
Experimentelle Kernphysik

Studies on Crossbar and Slotted Iris Structures for a Proton-Linear-Accelerator

W. Bauer, H. Eschelbacher, M. Kuntze

Gesellschaft für Kernforschung m.b.H.
Karlsruhe

1. Introduction

We are investigating the problems connected with a superconducting proton linac for several GeV [1]. As in the case of accelerators at room temperature we are interested in the usual features of rf-structures, i.e. high shunt impedance and large bandwidth. In addition we have to consider the mechanical fabrication taking into account superconductivity. In order not to complicate the deposition of superconducting material on the inner surface of the structure we believe, that a slotted iris structure might be preferred over a clover leaf structure, for instance.

To get an idea for our first experiment with a superconducting structure, which we hope to carry out in the next months, we did several experiments at room temperature. We started with some first measurements on a model of a slotted iris structure. Other measurements will follow. The aim of all measurements is to find the optimal geometrical parameters with respect to high shunt impedance and large bandwidth.

The slotted iris structure was designed for an operating frequency of 760 MHz. We report on measurements with two different cell lengths and various drift tube lengths. The Q-values were rather low due to the demountable model. Measurements on a model with higher Q-values are in preparation.

In another series of measurements we investigated a model of a cross bar structure, designed for an operating frequency of 357 MHz. These measurements were done for a comparison with an existing theory for the cross bar structure. We chose the mechanical parameters according to models used in the Rutherford Laboratory [16].

2. Evaluation of Experimental Data

Structures for the acceleration of charged particles are periodically loaded wave guides. With proper excitation one gets electromagnetic waves with axial field components within the guide, which have phase velocities lower than the velocity of light. In the following we will assume particles travelling along the guide on the symmetry axis (z-axis) with constant velocity v_p [2].

A structure can be strictly periodical only for a constant particle velocity. In order to be accelerated the particles have to take energy from the field. We will calculate the energy gain of the particles per unit length and derive a condition for acceleration.

To solve Maxwell's equations for homogeneous media (assuming infinite conductivity) we will write the field quantities by the following approximation, assuming J(x,y), G(x,y) independent of z

$$\mathcal{E}(x,y,z,t) = \mathrm{Re}\{J(x,y)\underline{\mathcal{E}}(z,t)\} = J(x,y)\ E(z)\cos(\omega t+\varphi) \quad (1)$$

$$\mathcal{H}(x,y,z,t) = \mathrm{Re}\{G(x,y)\underline{H}(z,t)\} = G(x,y)\ H(z)\sin(\omega t+\varphi) \quad (2)$$

where J(x,y), E(z), G(x,y) and H(z) are the absolute values of the coordinate functions of x, y, and z, respectively. φ is the phase of the electromagnetic wave, when the particle enters the cavity.

We start with eq. (1) and come to a differential equation for $\underline{\mathcal{E}}(z)$, which in general can be solved according Floquet's theorem for a strictly periodic structure. The solution is [3]

$$\underline{\mathcal{E}}(z) = \sum_{n=-\infty}^{+\infty} A_n e^{ik_n z} \cdot F(z) + \sum_{n=-\infty}^{+\infty} B_n e^{-ik_n z} \cdot F(-z) \quad (3)$$

where $k_n = \frac{2\pi}{\lambda_n}$ is the wave number for a wave propagating in plus or minus z-direction with amplitudes A_n and B_n, respectively. The coefficients $F(z) = F(z+L)$ are periodic functions with period L, if the structure consists of identical cells with cell length L. F(z) can be written as a Fourier expansion

$$F(z) = \sum_{m=-\infty}^{+\infty} b_m \exp\left(i \frac{2\pi m z}{L}\right) \tag{4}$$

Consider a periodic structure of length $l = N.L$. In order to have symmetry around $z = 0$ this structure consists of N-1 cells and half cells on each end. A structure with conducting end plates is a standing wave resonator. We take the standing wave case.

The boundary conditions are:

$$\left(\frac{d\mathcal{E}(z)}{dz}\right)_{z=o} = 0 \tag{5}$$

$$\left(\frac{d\mathcal{E}(z)}{dz}\right)_{z=l} = 0 \tag{6}$$

which includes

$$\left(\frac{\partial F}{\partial z}\right)_{z=o} = \left(\frac{\partial F}{\partial z}\right)_{z=l} = 0 \tag{7}$$

Eq. (5) gives $$A_n = B_n \tag{8}$$

The second boundary condition gives:

$$k_n \cdot L = \frac{n\pi}{N} \tag{9}$$

with $n = 0, 1, 2, \ldots\ldots$

$k_n \cdot L$ is the phase shift from cell to cell.

The sum over n (eq. (3)) indicates the possibility to excite the resonator with a discrete number of frequencies. λ_n is thus only given by the resonator length and is the length of the n-th wave in the guide. (Fig. 1) For a fixed wave number k_n, i.e. one excitation frequency at given resonator length the axial electric field is then given in terms of all possible m Harmonics of this frequency (so called "space harmonics"). The synthesis of these Harmonics creates the particular shape of the wave appropriate to the given structure. The points in the Brillouin diagram (Fig. 2) are given by eq. (9)

Taking only the normal modes restricts the range of the Brillouin diagram from $-\pi$ to $+\pi$. If we excite the resonator with the n = N'th wave, we get the π-mode.

Rewriting eq. (9) with $k_n = 2\pi/\lambda_n$ gives

$$l = n \cdot \frac{\lambda_n}{2} \tag{10}$$

where l = NL is the resonator length and λ_n is the chosen wave length within the resonator (Fig. 1). The wave length λ_1 is called the Fundamental wave length of the resonator.

Then the axial electric field within one resonator is given by a sum over the possible m Fourier components of the n^{th} Harmonics of the resonator.

$$E(z) = \sum_{m=-\infty}^{+\infty} a_m \cdot \cos\left([n+2mN]\,\frac{\pi z}{l}\right) = \sum_m a_m \cos\left(R\,\frac{\pi z}{l}\right) \tag{11}$$

with $R = n + 2mN$ and $a_m = 2A_n b_m$.

Along the tank the energy gain of a particle travelling in z-direction with velocity v_p is given by

$$W_T = e \cdot \int_0^{\ell} E(z) \cdot \cos(\omega t + \varphi)\, dz \tag{12}$$

where e = elementary charge.
The particle enters at time t = 0 the tank at the point z = 0, where the electromagnetic field has the phase ϕ. ϕ = 0 is taken at the crest of the field. In the particle coordinate system $t_p = z/v_p$ is the time of flight of the particle through the accelerator and ω is the frequency of a vacuum wave seen by the particle. ω is given by

$$\omega = 2\pi \frac{c}{\lambda_o} \tag{13}$$

where c = velocity of light and λ_o = vacuum wavelength. This results in the transformation

$$t_p = \frac{2\pi z}{\lambda_o \beta} \quad \text{with } \beta = \frac{v_p}{c} \tag{14}$$

Then the integral in eq. (12) is solved to give the energy gain per unit length

$$\frac{W_T}{\ell} = \frac{1}{2} \sum_m q_m \left[\frac{\sin\left(R\frac{\pi z}{\ell} + \frac{2\pi z}{\lambda_o \beta} + \phi\right)}{R\frac{\pi}{\ell} + \frac{2\pi}{\lambda_o \beta}} + \frac{\sin\left(R\frac{\pi z}{\ell} - \frac{2\pi z}{\lambda_o \beta} - \phi\right)}{R\frac{\pi}{\ell} - \frac{2\pi}{\lambda_o \beta}} \right]_{z=0}^{z=\ell} \tag{15a}$$

This can be written as

$$\frac{W_T}{\ell} = \sum_m \frac{q_m}{2} \left[\frac{\sin\left(\frac{\pi \ell}{\lambda_o \beta} + R\frac{\pi}{2}\right)}{\frac{\pi \ell}{\lambda_o \beta} + R\frac{\pi}{2}} \cos\left(\frac{\pi \ell}{\lambda_o \beta} + R\frac{\pi}{2} + \phi\right) + \frac{\sin\left(\frac{\pi \ell}{\lambda_o \beta} - R\frac{\pi}{2}\right)}{\frac{\pi \ell}{\lambda_o \beta} - R\frac{\pi}{2}} \cos\left(\frac{\pi \ell}{\lambda_o \beta} - R\frac{\pi}{2} - \phi\right) \right] \tag{15b}$$

The energy gain per unit length becomes maximal only if the argument of the sinus in the second term of eq. (15b) and at the same time the denominator vanishes. This gives the condition for acceleration

$$\lambda_o \beta = \frac{1}{R}\, 2\ell = \frac{2\ell}{n+2mN} \tag{16}$$

where for normal modes (m = 0) n is given by $n = \frac{\ell}{\pi} K_n$. For the π-mode is n = N.

The energy gain per unit length is given by

$$\frac{W_T}{\ell} = 1/2 \cdot a_o \cdot \cos \phi \qquad (17)$$

where

$$a_o = \frac{2}{\ell} \cdot \int_o^{\ell} E(z) \cdot \cos\left(\frac{R\pi z}{\ell}\right) \cdot dz \qquad (18)$$

with R = n+2mN.

The energy gain of a particle is sometimes written in another form. If the mean energy gain per unit length over one cell is defined as

$$\overline{W} = \frac{1}{L} \int_o^{L} E(z)dz \qquad (19)$$

and the Transit-time factor

$$T = \frac{\int_c^{L} (E(z) \cos\left(\frac{R\pi z}{\ell}\right)) dz}{\int_c^{L} E(z)\, dz} \qquad (20)$$

the whole energy gain is given by

$$W_T = N \cdot L \cdot \overline{W} \cdot T \cdot \cos \phi \qquad (21)$$

Eq. (22) and eq. (18) are equal. The particle velocity must be synchronous with the phase velocity of the excitation frequency according eq. (17). If the particle is riding on the crest of the wave, the maximum energy gain is called W_{To}. W_{To} is composed from the mean energy gain $\overline{W}$ and the Transit-time factor T. If the field has a phase shift Ø at the origin, the energy gain is lower and is called the real energy gain G.

$$G = W_{T_o} \cdot \cos \phi \qquad (22)$$

The efficiency of a resonator as a particle accelerating device is usually expressed in terms of the effective shunt impedance [4].

$$Z_{eff} = \frac{(\text{max. energy gain per unit length})^2}{\text{Power dissipated per unit length}} \qquad (23)$$

The resonator quality is given by the Q-factor

$$Q = \omega \frac{\text{stored energy}}{\text{power dissipation}} = \omega \cdot U/P \qquad (24)$$

With this definitions the ratio of Z_{eff} and Q becomes

$$\frac{Z_{eff}}{Q} = \frac{\overline{W}^2 \cdot T^2}{\omega \cdot U} \cdot \ell = \frac{\ell}{4\omega U} \left\{ \frac{2}{\ell} \int_0^{\ell} E(z) \cos\left(\frac{R\pi z}{\ell}\right) dz \right\}^2 \qquad (25)$$

This ratio is no longer depending on the power dissipation and therefore independent of the material of the resonator, the surface quality and the electrical contacts. It depends only on the geometry of the resonator. Z_{eff}/Q is proportional to ω, since $Q \sim \frac{1}{\sqrt{\omega}}$ and $Z_{eff} \sim \sqrt{\omega}$.

Z_{eff}/Q can be measured using perturbation techniques [5,6]. A bead of Volume V and dielectric constant ε_o is pulled along the z-axis. The resonance frequency shift Δf versus position z of the bead is measured. With Slater formula

$$\frac{\Delta f}{f} = -\frac{3}{4} \cdot \frac{V \cdot \varepsilon_o \cdot E(z)^2}{U} \qquad (26)$$

one gets

$$\frac{Z_{eff}}{Q} = \frac{8\pi}{3\omega^2 \cdot \varepsilon_o V \cdot \ell} \cdot \left[\int_o^{\ell} \sqrt{\Delta f} \cos\left(\frac{R\pi z}{\ell}\right) dz \right]^2 \qquad (27)$$

We calculated Z_{eff}/Q according eq. (27).

3. Slotted Iris Structure

3.1 General

The field configuration of a cylindrical wave guide is given in Fig. 3. The cylindrical wave guide is periodically loaded to get a phase velocity which is smaller than c, the velocity of light. Plotting frequency versus wave number k results in a characteristic curve, which is called the dispersion curve or Brillouin diagram [3, 7]. In a resonant cavity of length $(N \cdot L)$ there are $(N + 1)$ modes between 0 and π. Each mode is characterized by a certain phase shift $k_n L$ per cell which represents one point in the dispersion curve. The bandwidth of a resonant cavity is defined by the relative frequency difference of 0-mode and π-mode.

For a long accelerating structure with many modes the bandwidth is required to be as large as possible in order to obtain good mode separation and mode stability. In addition the rf-energy transport is enlarged through a steep dispersion curve and large bandwidth, respectively. The group velocity is given by the derivative of the dispersion curve. "Forward-wave" - $(v_{gr} > 0)$ and "backward-wave" - $(v^{gr} < 0)$ structures as distinguished in the travelling wave techniques have no special meaning in standing wave accelerators [8]. The normal iris structure is partitioned by conducting plates with central coupling holes. As shown in Fig. 4 the electric field is nearly unchanged by the coupling hole for 0-mode. For π-mode there is a large capacitive distortion, and the frequency of π-mode is increased with respect to the 0-mode frequency. The normal iris structure is a "forward-wave" structure. This structure has been extensively used in electron linear-accelerators [9].

For high energy proton linear accelerators, however, one has to lower the phase velocity by a large amount in order to accelerate protons of velocity v_p. The effective shunt impedance of an iris structure in this case becomes lower than

for other structures. In addition the requirements of beam dynamics to the coupling hole are somewhat contradictory to the requirements of rf-techniques.

For a slotted iris structure the effective shunt impedance is increased with respect to an iris structure due to better coupling. Fig. 5 shows an iris structure with small coupling slots for inductive coupling in direction of the magnetic field. Fig. 6 gives a picture of the coupling slots only. The frequency of 0-mode is not influenced by the slots, because there are no radial currents in the wall to be disturbed by the slots. But for π-mode the resonance frequency is decreased because currents are disturbed by the coupling slots and the effective inductivity is increased. The slotted iris therefore has a "backward-wave" characteristic [8]. In the slotted iris and the normal iris-structure one can excite the normal modes with wave-numbers between $k = 0$ and $k = \pi/L$.

3.2 Description of the Model

Table I shows the relevant mechanical data for the slotted iris structure. Fig. 7 is an outline of our demountable model, which consisted of brass plates and brass cylinders.

Tank diameter, plate thickness and slot angle were fixed parameters. In addition the drift tube diameter and the beam aperture were constant throughout the measurements. The cell length L was chosen according the condition for acceleration eq. (16) in the π-mode.

We measured models of two different cell lengths and chose an operating frequency of 760.000 MHz. At this frequency $L = 9.85$ cm corresponds to $\beta = 0.5$ (i.e. a proton energy of 145 MeV), and $L = 17.75$ cm corresponds to $\beta = 0.9$ (i.e. a proton energy of 1200 MeV).

For each cell length we varied the drift tube length in several steps. For each drift tube length we increased the slot width starting near the outer wall of the cylinder in several steps down to the diameter of the drift tube.

In models of different numbers of cells we measured the distribution of the axial electric field for the π-mode and the resonance frequency of different modes to get the Brillouin diagram. We calculated from our experimental data the effective shunt impedance over Q (according eq. 27) and the bandwidth of the slotted iris structure.

In addition we measured the Q-values, in some cases.

3.3 Experimental Arrangement

To measure Z_{eff}/Q according to the well known method introduced by J.C. Slater [5] we used a rf-generator Schomandl decade) and a microamperemeter to indicate the resonance maximum (Fig. 8). For all measurements we used the same positions of the coupling loops, the same brass bead (Ø 10 mm) and Nylon thread (Ø 1 mm). The room was temperature stabilized. Yet the error of the measured resonance frequency shifts is about $\pm$ 2 kHz, which corresponds to an error in Z_{eff}/Q nearly 5%. This is due to the uncertainty in finding the resonance maximum with models of moderate Q-values. The accuracy of these measurements has been increased using a lock-in oscillator in the range of 600 to 800 MHz as for the Crossbar structure discussed below.

3.4 Experimental Results for the Slotted Iris Structure

Fig. 9 gives the dispersion curve of the slotted iris structure with cell length L = 9.85 cm. There are four families of curves for different ratios of gaplength over cell length g/L. Parameter is the slot width (mm).

For g/L = 1 (no drift tubes) the largest bandwidth does not occur for the biggest slotwidth. The bandwidth for a slot width of 1 cm, 5 cm and 8 cm is substantially lower than for a slotwidth of 3 cm. The same but less pronounced can be seen at different values of g/L. Increasing the slot width, that means primarily, making the coupling stronger, gives not always higher band width. The reason for this may be, that near the center of the resonator the electric field participates more and more in coupling, increasing the π-mode frequency [10]. This effect is strongest without drift tubes.

The best values of bandwidth we obtained with slotted iris structure are about 9%.

The resonance frequency of the π-mode is strongly influenced by the geometry. Changing only the drift tube length in a fixed model changes the resonance frequency in the range of 600 MHz to 800 MHz. Thus for a given cell length by changing the drift tube length ß is varied. In addition we found the resonance frequency nearly independent of the slot width. However, Z_{eff}/Q is strongly influenced by the slot width.

Fig. 10 summarizes our experimental results for resonance frequency versus $ß = 2L.\nu/c$ for different drift tube length and a slot width of 8.3 cm. Fig. 11 gives the equivalent results for a slot width of 4.0 cm. According to two different cell lengths we have two families of points which cluster around ß = 0.5 and ß = 0.9.

Fig. 12 and Fig. 13 give the values of Z_{eff} versus ß as deduced from the bead measurements for different cell length and a slot width of 8.3 cm and 4.0 cm, respectively.

The measured Q-values were scaled proportional to $\frac{1}{\sqrt{\omega}}$ with respect to 760 MHz and multiplied by a factor of two, due to the different conductivity of brass and copper.

In this first measurement at room temperature we looked for a relative optimalization of shunt impedance with respect to the mechanical data. Therefore we had no optimalized Q-values. The measured Q-values of the slotted iris structure vary from 6000 at a cell length of L = 9.85 cm to 10 000 at L = 17.75 cm. We interpolated linearly between the measured numbers.

In a superconducting experiment we will probably use a different mechanical model. Measurements on such a model, which will certainly have higher Q-value, are in preparation. In Tab. II all experimental data are summarized.

4. Cross Bar Structure

4.1 General

The cross bar structure is an improvement derived from the Alvarez-type of drift tube structures [11, 12, 13, 14]. Considering a rectangular wave guide periodically loaded with parallel stems (Fig. 14) the distribution of the electric and magnetic fields in the guide is easily given. This distribution is like the typical distribution of fields in a coaxial resonator and is shown in Fig. 15 for the 0-mode and the π-mode. For a rectangular wave guide the resonance frequencies of the 0-mode and the π-mode are equal, because the frequency is determined by $\lambda_o/2$ (Fig. 14). λ_o is the vacuum wave length. The dispersion curve (Fig. 16) is a horizontal line. Changing this rectangular structure by three steps to its final geometry, one gets by each step either an increase of 0-mode frequency or a decrease of π-mode frequency, schematically shown in Fig. 16 and described in the following.

1. Rounding the corners results in a cylindrical wave guide, disturbs above all the magnetic field in the 0-mode. This increases the 0-mode frequency and has no influence on the π-mode frequency.

2. Introducing drift tubes to the parallel stems one mainly disturbs the axial electric field of the π-mode, resulting in a decrease of the π-mode frequency.

3. Introducing stems with very short drift tubes situated rectangular to the original stems, effects a further decrease of the π-mode frequency.

The final structure shows Fig. 17.

In comparison to the slotted iris structure the dispersion curve of the crossbar structure shows a much larger width of the passband. This is due to the different coupling. One single cell of length L in the cross bar structure for instance is not partitioned by conducting plates like in the slotted iris structure, therefore in the cross bar structure one can excite modes with wave numbers between $k = 0$ and $k = 2\pi/L$. Thus, the mode with the best conditions concerning mode separation and mode stability is the π-mode, while it will be the π/2-mode for the slotted iris structure. In a cross bar model consisting of two cells one can find three modes, the π/2-, π- and 3π/2-mode.

The typical measurement of the resonance frequency shift versus position z of the bead is shown in Fig. 18 and Fig. 19. From this method no information is obtained about the sign of each peak. The mode is determined by the resonance frequency. For the cross bar structure the 0-mode has the highest frequency, the π-mode frequency is definitely lower.

4.2 Description of the Model

The Crossbar model was machined of brass and consisted of four single rings (Fig. 14) joined together with indium wire to have good electrical contact. We could easily exchange the long drift tubes screwed into the stems. Coupling loops were situated near those stems, which carry current in the π-mode.

The mechanical data for the Crossbar structure are listed again in Table I. Tank diameter, stem diameter and drifttube shape were chosen according A. Carne [16]. We measured a two cell model with only one cell length of L = 21 cm, which corresponds at $\beta = 0,5$ to a resonance frequency of 357,000 MHz.

Within one cell length L we have two gaps of gaplength g/2 and two kinds of drifttubes (Fig. 14). All stems had the same diameter. The length of the short drifttubes equals the stem diameter. We varied the length of the long drifttubes in several steps, thus variing the gaplength. The idea was to change only one geometrical parameter and keep constant all the others. This is of special interest for a comparison with a theoretical treatment of the Crossbar structure given by G. Dome[15].

We studied two different drifttube shapes: In one series of measurements we used drifttubes of nine different length with rounded corners, in the other we tested five different drifttube length with flat fronts.

4.3 Experimental arrangement

The experimental arrangement for the measurement of Z_{eff}/Q was as follows (Fig. 20). We connected a 60 dB amplifier with a bandwidth of about 100 kHz to the cavity to have positive feedback. The amplifier worked as a lock-in-oscillator at the π-mode frequency and followed the frequency deviations due to the brass bead pulled along the axis. The central frequency of the amplifier was adjustable between 300 and 600 MHz. With this arrangement the frequency is read by an accuracy better than $\pm$ 100 Hz. Therefore Z_{eff}/Q could be calculated with a mean square deviation of 0,5 %. We found, that this method is about ten times more accurate than using a RF-generator and an indicator for the resonance maximum.

4.4 Experimental results for the cross bar structure

We measured in a two cell cross bar model the resonance frequencies of the three existing modes. Fig. 21 gives a summary of this frequency measurements on the cross bar model with rounded drift tubes. Frequency versus mode is shown in form of the dispersion curve with gap length over cell length as parameter. From this crude Brillouin diagram we could not determine the bandwidth. In addition the 0-mode frequency is not measurable in the cross bar structure. But what one can see from Fig. 21 is that the bandwidth does not depend very much on the gap length. The π-mode frequencies increase nearly linear with g/L. The reason for this may be that the axial electric field is more disturbed if the drift tubes are longer.

We have calculated the values of π-mode frequencies from the formula given by G. Dome. Fig. 22 is a plot of frequency versus gap length of our experimental data. For π-mode the measured figures are about 5% lower than the calculated values.

From the bead measurements we deduced Z_{eff}/Q according Eq.(27) only for the π-mode.

For the cross bar structure we chose 357 MHz as operating frequency and scaled the values Z_{eff}/Q proportional to ω.

The measured mean Q-value is scaled proportional to $\frac{1}{\sqrt{\omega}}$ and multiplied by a factor of two, due to the different conductivity of brass and copper. We derived $Q = 5200$.

In Fig. 23 Z_{eff}/Q versus g/L for two series of measurements (with flat fronted drift tubes and with round cornered drift tubes) is given. For comparison the third curve is calculated according G. Dome [15]. The agreement is reasonable.

All experimental data are summarized in Tab. III.

5. Discussion

For a given structure we want an optimalisation of shunt-impedance with respect to the geometrical parameters. For this purpose we must know the dependence of shuntimpedance on different geometrical parameters. In first step we have looked for the influence of the drift tube length on the shuntimpedance.

There holds an acceleration condition between the wavelength of the guide λ_g and the wavelength λ_o of the excitation frequency, if the structure is used for the acceleration of charged particles.
In π-mode there is

$$\lambda_g = \lambda_o \beta = 2L \qquad (16)$$

where $\beta = v_p/c$ and L = cell length.

We discuss the measurements on the slotted iris structure first:
For a constant cell length L the resonance frequency c/λ_o is varied by changing the drift tube length . This results in different β's. On the other hand particles should be accelerated with one excitation frequency along the whole linac. To bring the frequencies for different drift tube length to the same frequency, we could have changed some other geometrical parameter simultaneously, for instance the cell length.

We did not do this experimentally, but deduced it from our experimental results utilizing the frequency dependence of the parameters. We therefore scaled to one frequency by multiplying the cell length, used in the measurements, with a factor f_n/f_o, where f_n is the measured resonance frequency and f_o = 760 MHz is the excitation frequency. The measured shunt-impedances were scaled too. The scaling factor is $\sqrt{f_o/f_n}$.

Figs. 12 and 13 (for two different slot widths) show shunt-impedance, scaled to 760 MHz versus ß. To each point in Figs. 12 and 13 there belongs a different cell length.

By drawing lines at ß's of 0.3, 0.5, 0.7 and 0.9 (dotted lines in Figs. 12 and 13) we can draw curves of shuntimpedances versus drift tube length for constant ß as shown in Fig. 24 (slot width 8,3 cm) and Fig. 25 (slot width 4,0 cm). Along the curves of constant ß each point corresponds to a different cell length (Fig. 12 and 13) and therefore to a different frequency.

We now need lines of constant frequency, which we may sketch from the frequency versus ß curves (Figs. 10 and 11). By drawing lines at constant frequency and interpolating between the measured drift tube lengths at ß = 0.3, 0.5, 0.7 and 0.9 we get the crosspoints of lines with constant ß and lines with constant frequency. The lines with constant frequency are given in Figs. 24 and 25 as dotted lines.

Between ß = 0.3 and 0.9 we deduced from the measurements with a tank diameter of 28,3 cm and the original set of drift tubes the highest shuntimpedances at 710 MHz. But we want this optimal shuntimpedances at 760 MHz, so we have to scale down all geometrical parameters simultaneously by the factor 710/760 . This results in a tank diameter of 26,9 cm. The drift tube length is scaled down proportionately.

For 760 MHz and a tank diameter of 26,9 cm we got the following result (drift tube lengths are scaled):

ß	L cm	drift tube length cm slot width 4,0 cm	drift tube length cm slot width 8,3 cm	Z_{eff} [MΩ/m] slot width 4,0 cm	Z_{eff} [MΩ/m] slot width 8,3 cm
0,3	5,93	1,3	2,9	9,0	14,6
0,5	9,88	2,3	3,5	11,7	15,9
0,7	13,81	3,6	4,4	14,1	16,4
0,9	17,75	5,5	6,0	14,3	17,6

Fig. 26 summarizes our results of shuntimpedances versus ß, as deduced from the variation of drift tube length. There may be a maximum error of ± 10 % in shuntimpedance due to the measurements of Q and the interpolation of drift tube lengths.

The shuntimpedance increases with increasing ß and is higher for bigger slot width. We compare our results on the slotted iris structure with the figures given by Giordano [17], who investigated models of slotted iris structure with nearly equal cell length, tank diameter, slot width and drift tube length, but different diameter of the bore holes.

From Figs. 24 and 25 it can be seen, that the shuntimpedance increases by a factor of two from drift tube length 0 cm to 6,5 cm in the original measurements. For a slot width of 8,3 cm there seems to be a maximum in shuntimpedance for a drift tube length of 4,0 cm. This is not yet well understood.

In comparison to Giordano we did not get a decrease in shuntimpedance at very long drift tubes. Giordano's measurements show a decrease of this effect with decreasing bore hole diameter. As we choose a very small bore hole diameter in our model our result seems to be reasonable. We will investigate this point further.

For the measurements on the cross bar structure the situation was similar. Changing the drift tube length gives different resonance frequencies. This results in slightly different ß's, if the cell length is constant.

But in the case of the cross bar structure we did not look for optimal shuntimpedances. However, we scaled the measured values of Z_{eff}/Q by multiplying with a factor $357/f_n$, where f_n was the measured resonance frequency. Fig. 23 shows Z_{eff}/Q, scaled to 357 MHz versus g/L, the ratio of gaplength to cell length. Z_{eff}/Q increases with increasing length of the long drift tube, i.e. with decreasing g/L. The two series of measurements with flat fronted drift tubes and with round cornered drift tubes gave similar results. Both experimental curves lie slightly

higher than the curve calculated according to G. Dome's theory. Since the main purpose of the cross bar measurements was the comparison with the theory, we did not measure different cell lengths (as in the case of the slotted iris structure) and therefore did not get the ß-dependance of shuntimpedance.

Literature

[1] H. Schopper: Minutes of the Conference on Proton Linear Accelerators, MURA, July 1964, p. 108.

[2] W.K.H. Panofsky: Linear Accelerator Beam Dynamics, UCRL-1216 (1951).

[3] L. Brillouin: 'Wave Propagation in Periodic Structures', Dover Publications (1953).

[4] E.A. Knapp: Minutes of the Conference on Proton Linear Accelerators, Yale, Oct. 1963, p. 131.

[5] J.C. Slater: 'Microwave Electronics' D. Van Nostrand Comp., New York (1950).

[6] L.C. Maier, J.C. Slater: 'Field Strength Measurements in Resonant Cavities', Journ. Appl. Phys., 23 (1952)

[7] L. Brillouin: Journ. Appl. Phys. 19, 1023 (1948).

[8] M. Chodorow, R.A. Craig: Proc. I.R.E. (Aug. 1957) p. 1106

[9] P.T. Demos, A.F. Kip, J.C. Slater: 'The M.I.T. Linear Electron Accelerator', Journ. Appl. Phys. 23, (1952)

[10] S. Giordano: Minutes of the Conference on Proton Linear Accelerators, Yale, Oct. 1963, p. 153

[11] A. Carne: Conference Dubna, USSR (Aug. 1963).

[12] A. Carne: Minutes of the Conference on Proton Linear Accelerators, Yale, Oct. 1963, p. 104

[13] A. CArne: Minutes of the Conference on Proton Linear Accelerators, MURA, July 1964, p. 1

[15] G. Dome: V. International Conference on High Energy Accelerators, Frascati (Italy), 1965.

[14] A. Carne: P.L.A. Progress Report 1964, NIRL/R/81,p.20.

[16] A. Carne: Ruth. Lab. private communication.

[17] S. Giordano: Minutes of the 1964 Conference of Proton Linear Accelerators, MURA, p. 60.

T a b l e I

Mechanical Data

	Slotted Iris (mm)	Crossbar (mm)
cell length (L)	98.5 178.0	210
tank diameter	288	280
stem "	-	21
drift tube "	65	65
beam aperture	17.5	17.5
drift tube length	65 - 16	125 - 61
slot angle	44^{o}	
slot width	10 - 83	
plate thickness	6	

T a b l e II

Experimental results for slotted iris structure

a.) slot width 8,3 cm:

drift tube length [cm]	frequency [MHz]	ß	Zeff/Q [kΩ/m]	Q	Zeff [MΩ/m]	T
0	771,655	0,500	1,17-5%	7000	8,2	0,730
	780,816	0,920	1,16	10100	11,7	0,689
1,6	754,991	0,495	1,64	6950	11,4	0,716
	771,458	0,915	1,24	10100	12,6	0,695
2,6	736,358	0,480	2,02	6850	13,8	0,754
	760,715	0,902	1,38	10000	13,8	0,688
3,6	711,474	0,470	2,31	6800	15,7	0,807
	746,506	0,880	1,71	9900	17,0	0,712
5,3	661,147	0,430	2,59	6450	16,4	0,868
	719,690	0,850	1,70	9650	15,7	0,764
6,5	596,828	0,390	2,81	6190	17,4	0,915
	688,158	0,810	1,88	9360	17,6	0,810
9,6	604,744	0,710	2,38	8600	20,5	0,890
11,8	540,840	0,640	2,36	8100	19,1	0,943

b.) slot width 4,0 cm:

drift tube length [cm]	frequency [MHz]	ß	Zeff/Q [kΩ/m]	Q	Zeff [MΩ/m]	T
0	728,515	0,480	1,05	6850	7,2	0,733
	752,918	0,890	1,00	9950	10,0	0,693
1,6	718,386	0,470	1,46	6800	9,9	0,716
	747,073	0,886	1,13	9900	11,2	0,696
2,6	705,859	0,460	1,74	6700	11,7	0,755
	739,858	0,878	1,33	9850	13,1	0,699
3,6	687,676	0,450	2,00	6600	13,2	0,803
	729,549	0,860	1,46	9750	14,2	0,720
5,3	647,294	0,430	2,32	6450	14,9	0,870
	708,970	0,840	1,51	9600	14,5	0,770
6,5	594,876	0,390	2,55	6190	15,8	0,925
	682,899	0,810	1,57	9360	14,7	0,810
9,6	607,741	0,720	2,12	8700	16,9	0,895
11,8	546,299	0,650	2,14	8250	17,6	0,936

c.) slot width 5,0 cm:

drift tube length [cm]	frequency [MHz]	ß	Zeff/Q [kΩ/m]	Q	Zeff [MΩ/m]	T
0	740,635	0,48	1,03	6850	1,7	0,736
3,6	696,813	0,46	2,03	6700	13,6	0,804
6,5	597,915	0,36	2,64	6190	16,3	0,924

d.) slot width 3,0 cm:

drift tube length [cm]	frequency [MHz]	ß	Zeff/Q [kΩ/m]	Q	Zeff [MΩ/m]	T
0	731,512	0,48	0,94	6850	6,4	0,716
3,6	692,565	0,45	1,94	6600	12,8	0,801
6,5	600,867	0,39	2,39	6190	13,9	0,919

T a b l e III

Experimental results for crossbar structure

a.) round cornered:

g/L	frequency MHz	ß	Zeff/Q ±0,5%	T
0,30	345,947	0,484	2,119[$\frac{k\Omega}{m}$]	0,901
0,34	357,409	0,500	2,033	0,872
0,38	369,261	0,517	1,992	0,868
0,42	380,674	0,533	1,824	0,838
0,46	398,422	0,558	1,683	0,833
0,50	404,166	0,566	1,656	0,812
0,54	416,062	0,582	1,515	0,789
0,58	428,396	0,600	1,416	0,756
0,62	440,434	0,615	1,306	0,740

b.) flat fronted:

g/L	frequency MHz	ß	Zeff/Q ±0,5%	T
0,30	336,704	0,472	2,129[$\frac{k\Omega}{m}$]	0,909
0,38	363,859	0,510	1,928	0,864
0,46	383,957	0,538	1,758	0,844
0,54	407,528	0,750	1,580	0,785
0,62	431,964	0,605	1,415	0,732

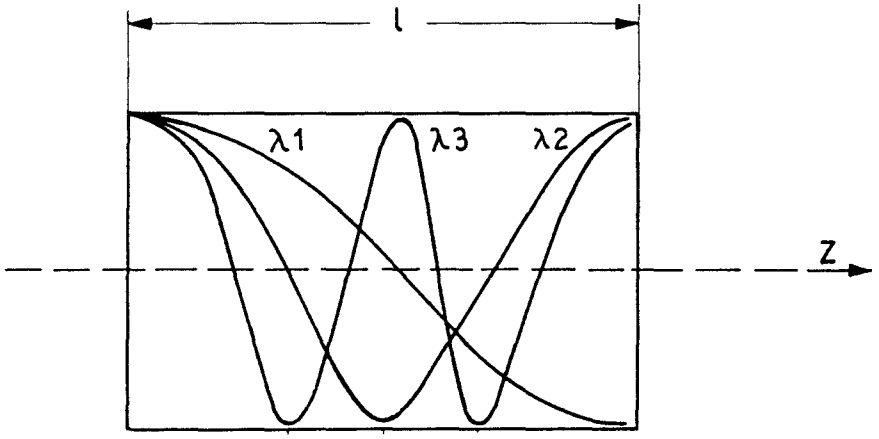

Fig. 1

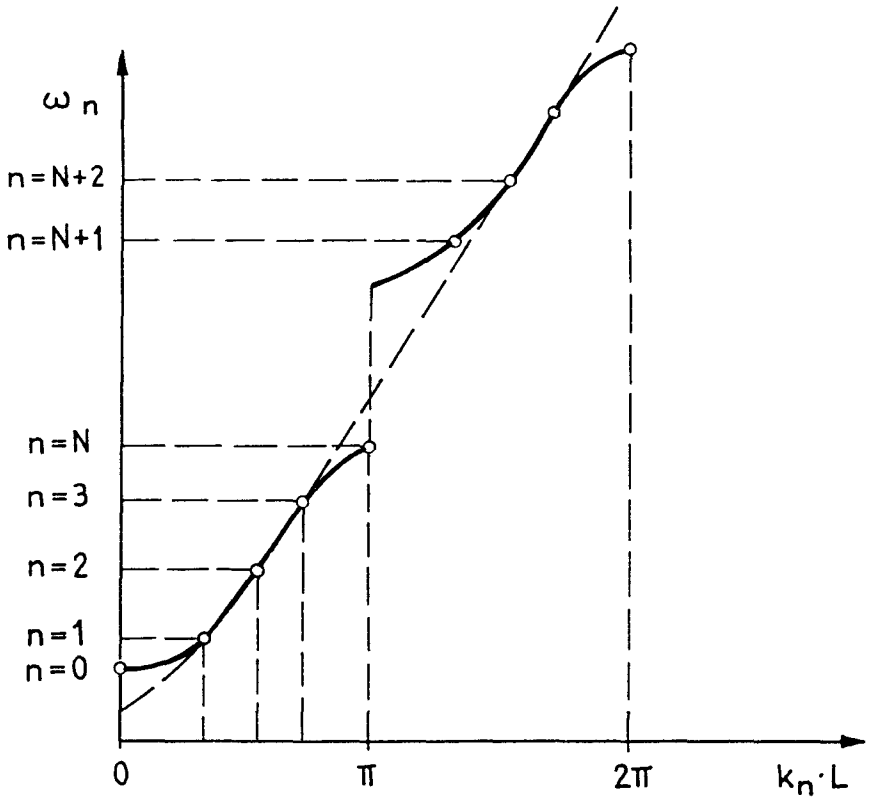

Fig. 2

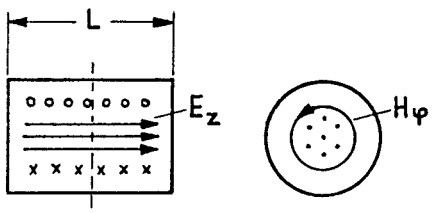

Fig. 3 TM 010 mode in cyl. resonator

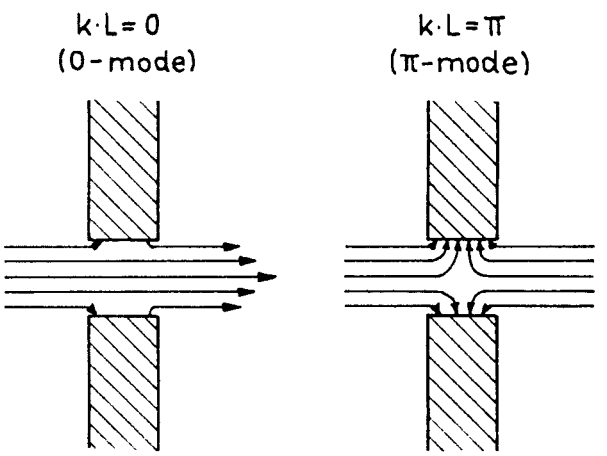

Fig. 4 Influence of beam hole on axial E-field

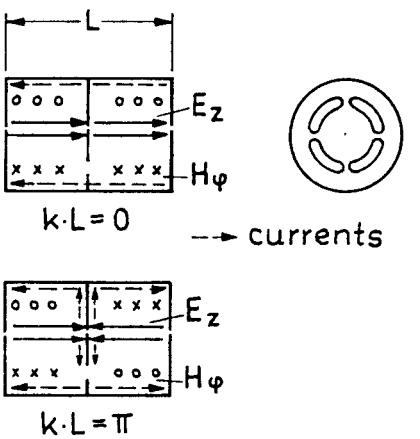

Fig. 5 Iris with coupling-slots for H-field

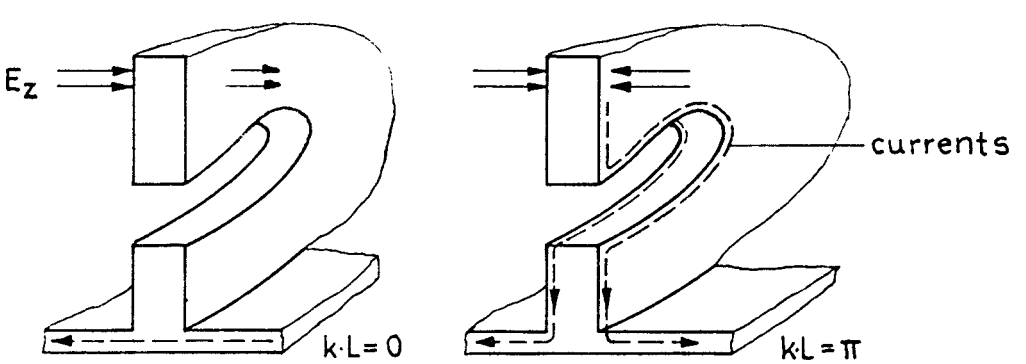

Fig. 6 Influence of slots on the current in the plates

Fig. 7

Slotted Iris-Model

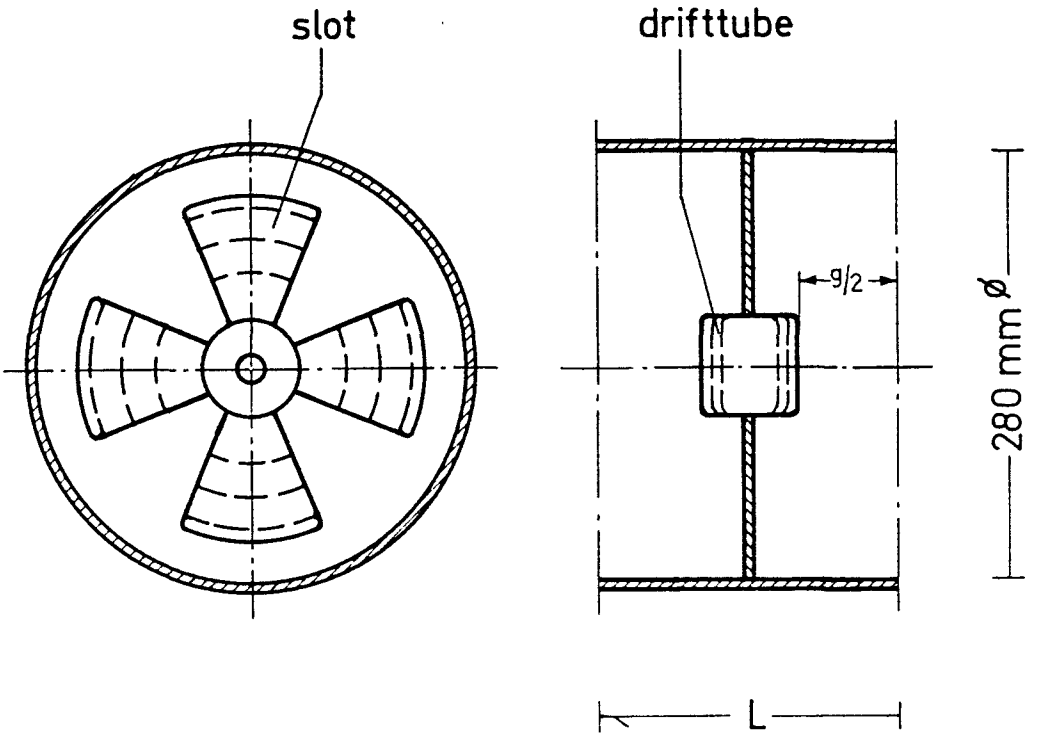

dotted lines show the variation of drifttube length and slotwidth

Fig. 8 Slotted Iris Measurements

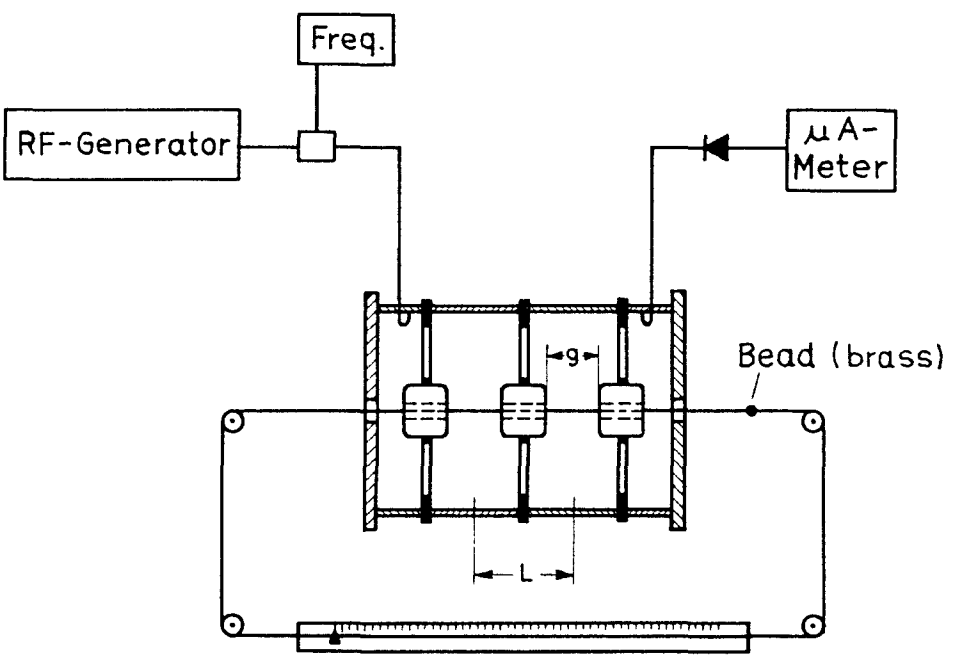

Fig. 9 Slotted Iris (L = 9.85 cm)

(Dispersion curve)

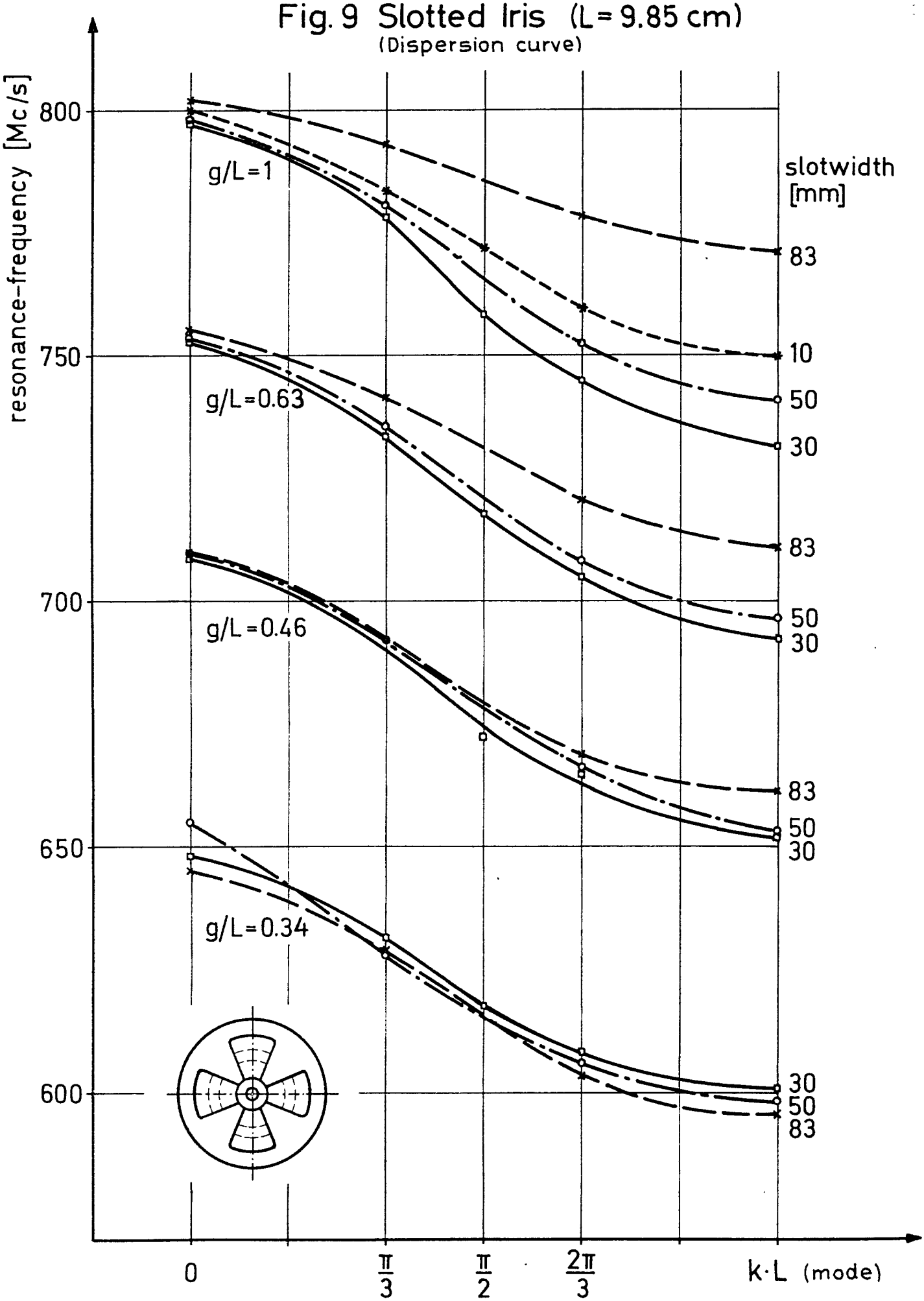

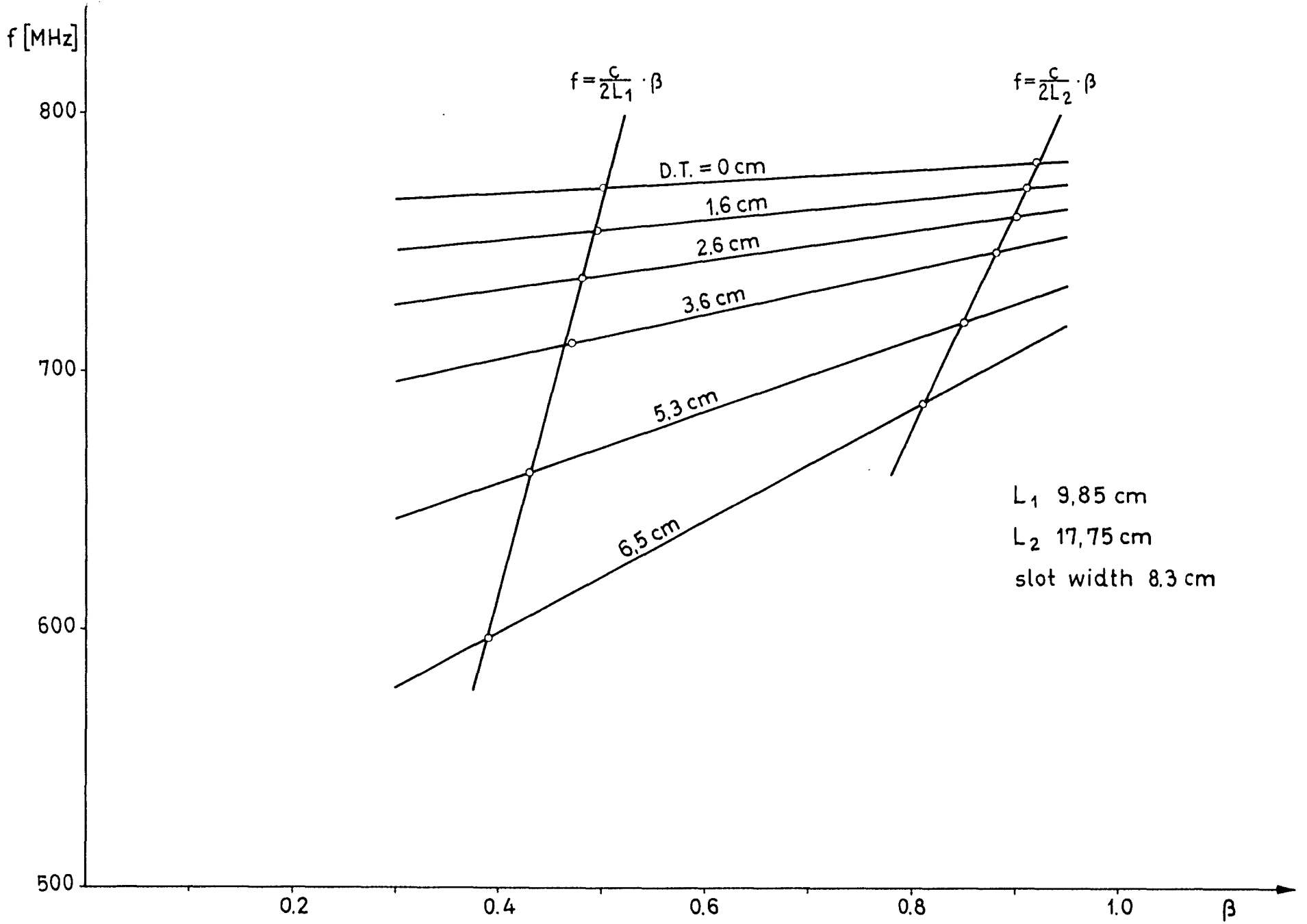
f [MHz]
800
700
600
500
0.2
0.4
0.6
0.8
1.0
β
$f=\frac{c}{2L_1}\cdot\beta$
$f=\frac{c}{2L_2}\cdot\beta$
D.T. = 0 cm
1.6 cm
2.6 cm
3.6 cm
5.3 cm
6.5 cm
L_1 9,85 cm
L_2 17,75 cm
slot width 8.3 cm

Fig. 10

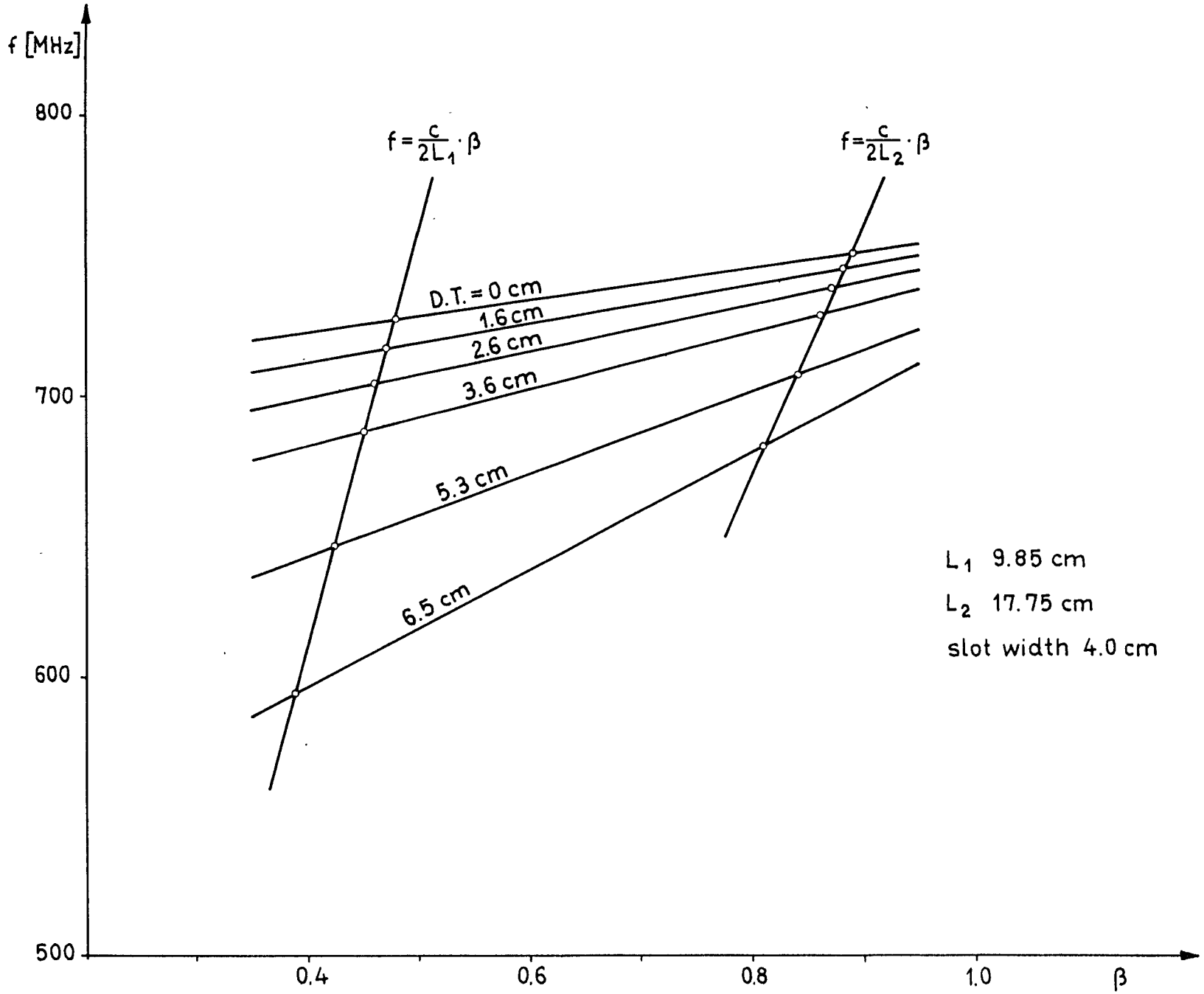
f [MHz]
800
700
600
500
0.4
0.6
0.8
1.0
β
$f = \frac{c}{2L_1} \cdot \beta$
$f = \frac{c}{2L_2} \cdot \beta$
D.T. = 0 cm
1.6 cm
2.6 cm
3.6 cm
5.3 cm
6.5 cm
L_1 9.85 cm
L_2 17.75 cm
slot width 4.0 cm

Fig. 11

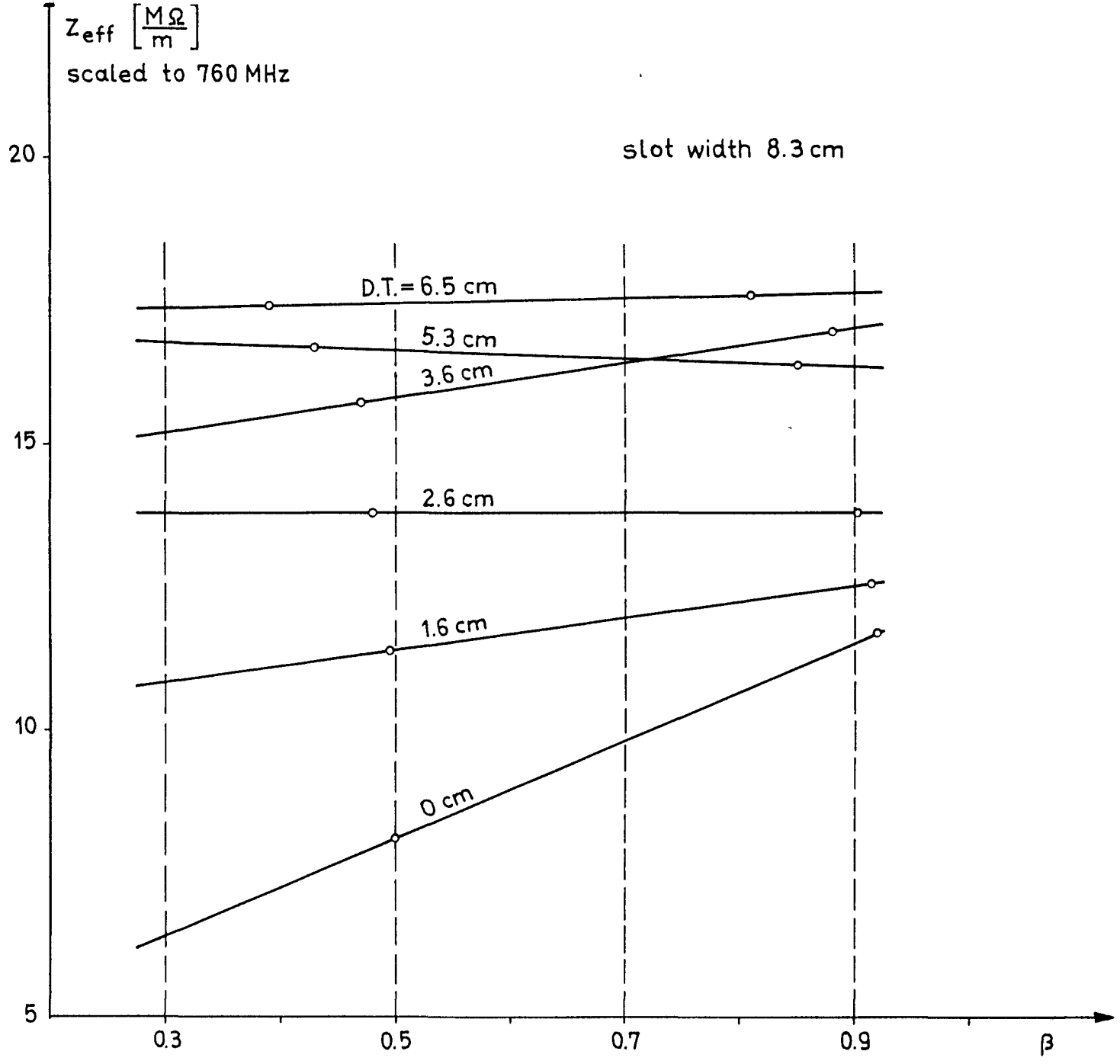
Z_{eff} $\left[\frac{M\Omega}{m}\right]$
scaled to 760 MHz
slot width 8.3 cm
20
15
10
5
D.T. = 6.5 cm
5.3 cm
3.6 cm
2.6 cm
1.6 cm
0 cm
0.3
0.5
0.7
0.9
β

Fig. 12

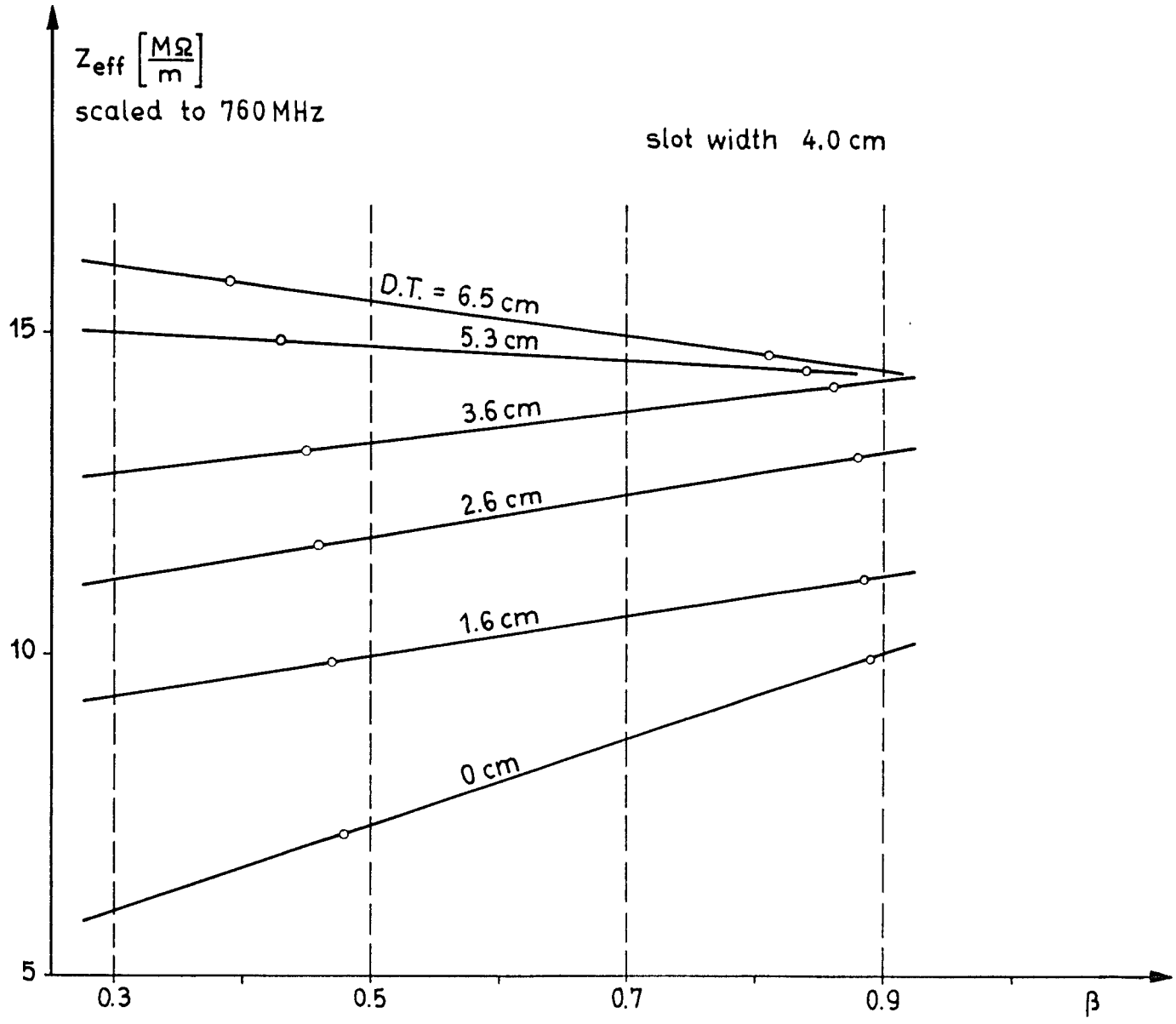
$Z_{eff}\left[\frac{M\Omega}{m}\right]$
scaled to 760 MHz
slot width 4.0 cm
D.T. = 6.5 cm
5.3 cm
3.6 cm
2.6 cm
1.6 cm
0 cm
15
10
5
0.3
0.5
0.7
0.9
β

Fig. 13

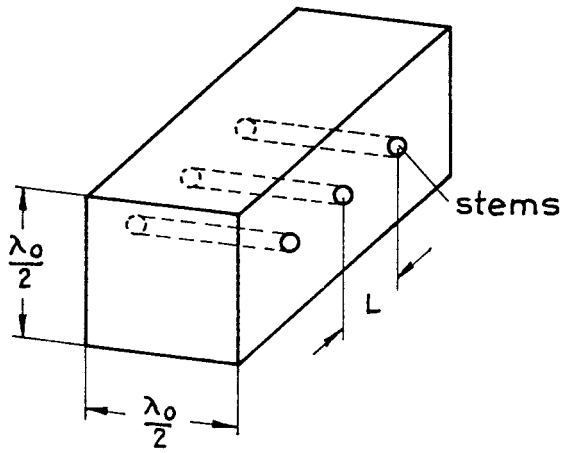

Fig. 14 Periodically loaded rectangular waveguide

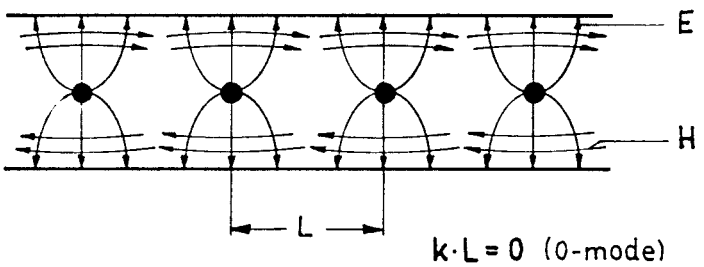

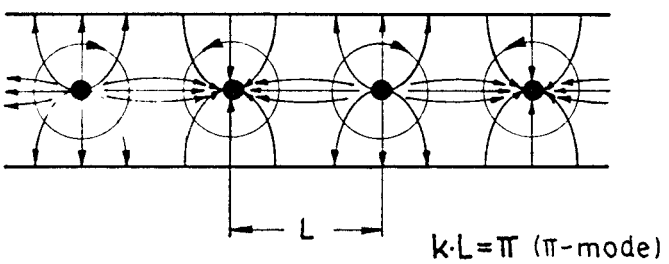

Fig. 15 Distribution of E- and H-fields in a waveguide shown in Fig. 9

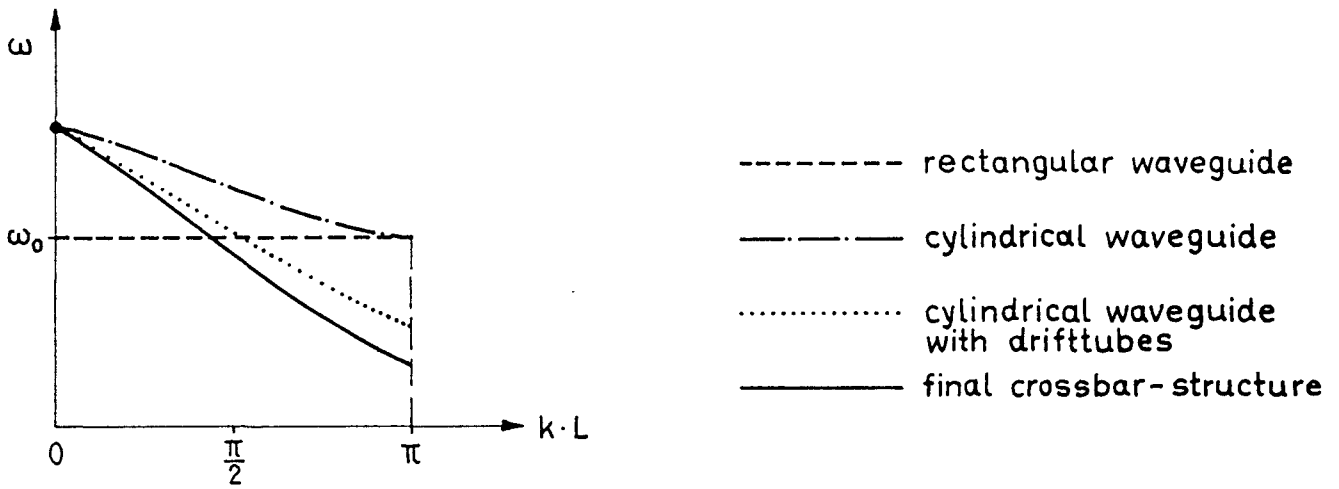

Fig. 16 Dispersion curve of crossbar-structure

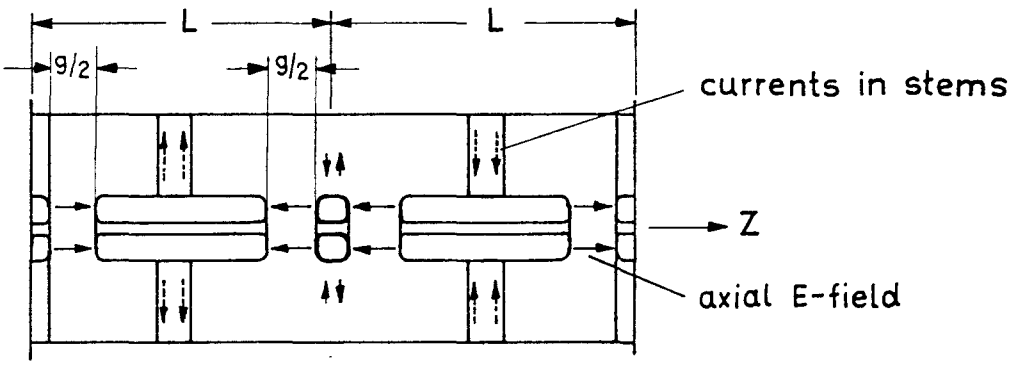

Fig. 17 Crossbar-structure
(fields and currents in π-mode)

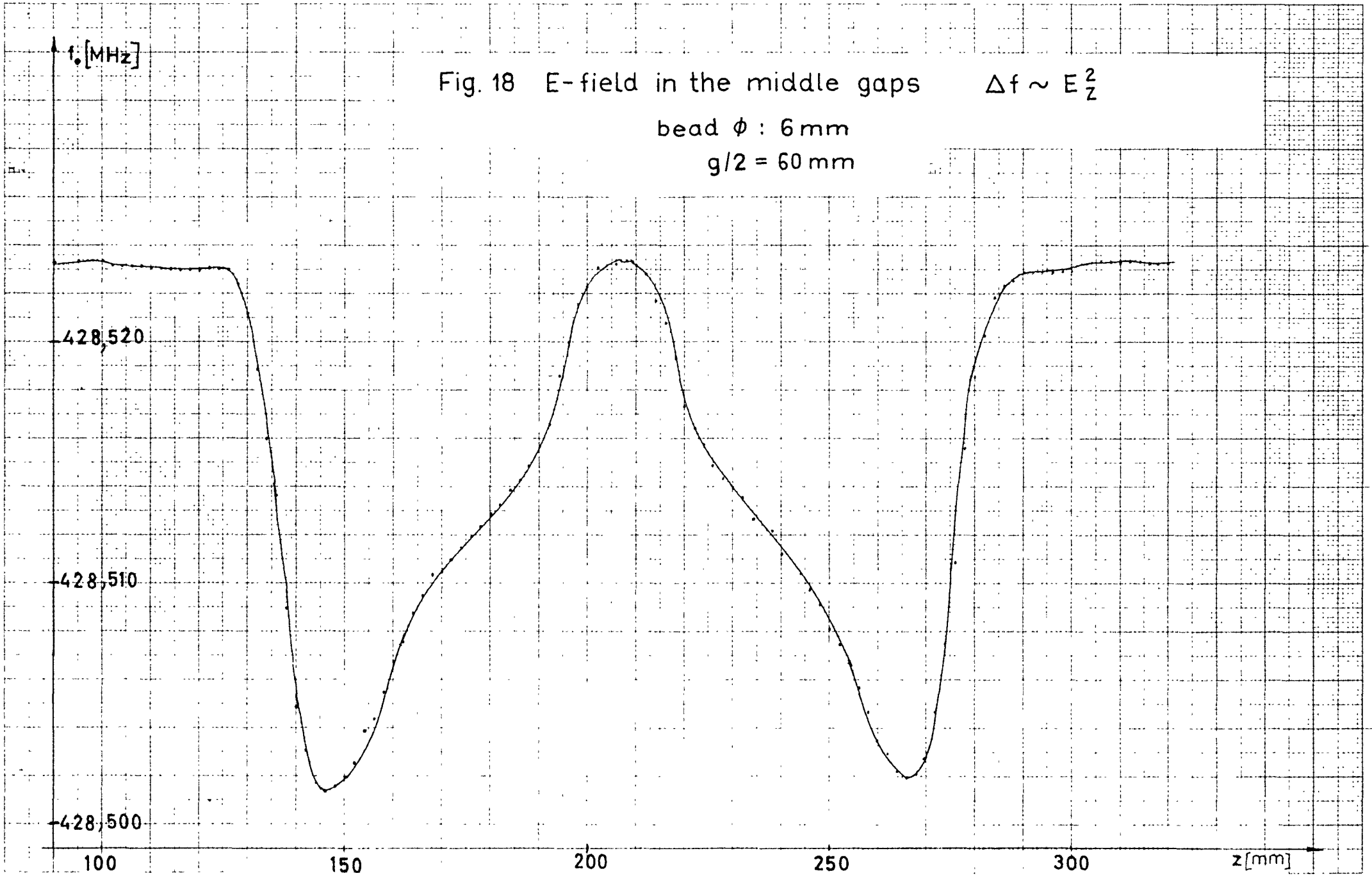

Fig. 18 E-field in the middle gaps $\Delta f \sim E_z^2$

bead ϕ : 6 mm

g/2 = 60 mm

Fig.19 Cross-Bar
field distribution
drift tubes with flat fronts

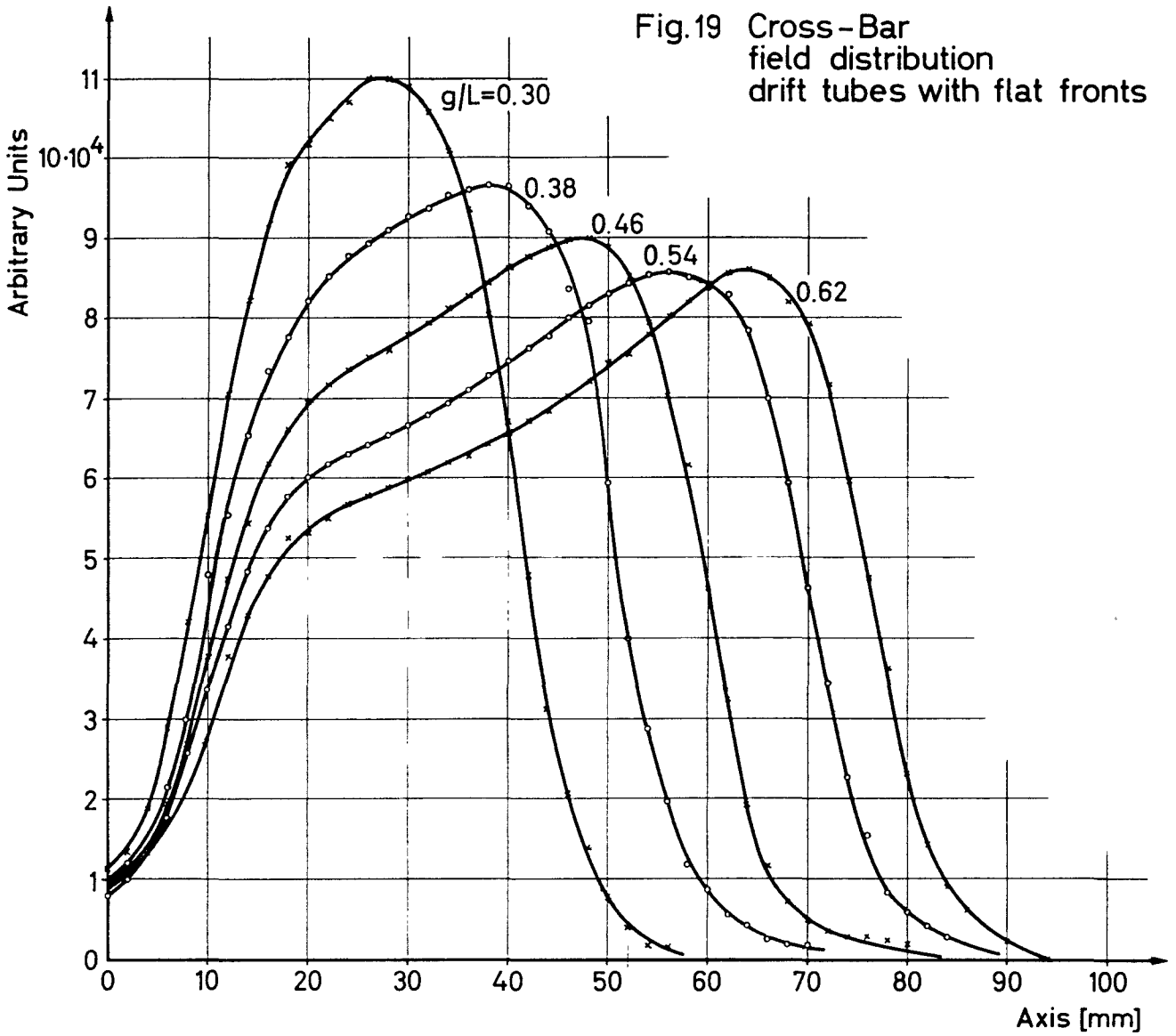

Fig.20 Crossbar Measurements

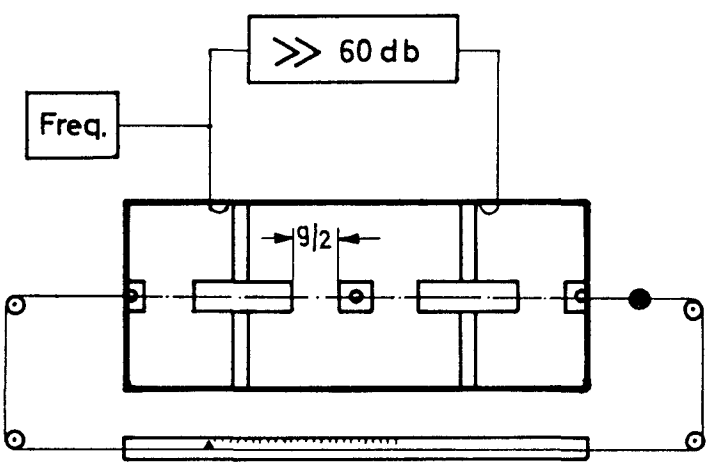

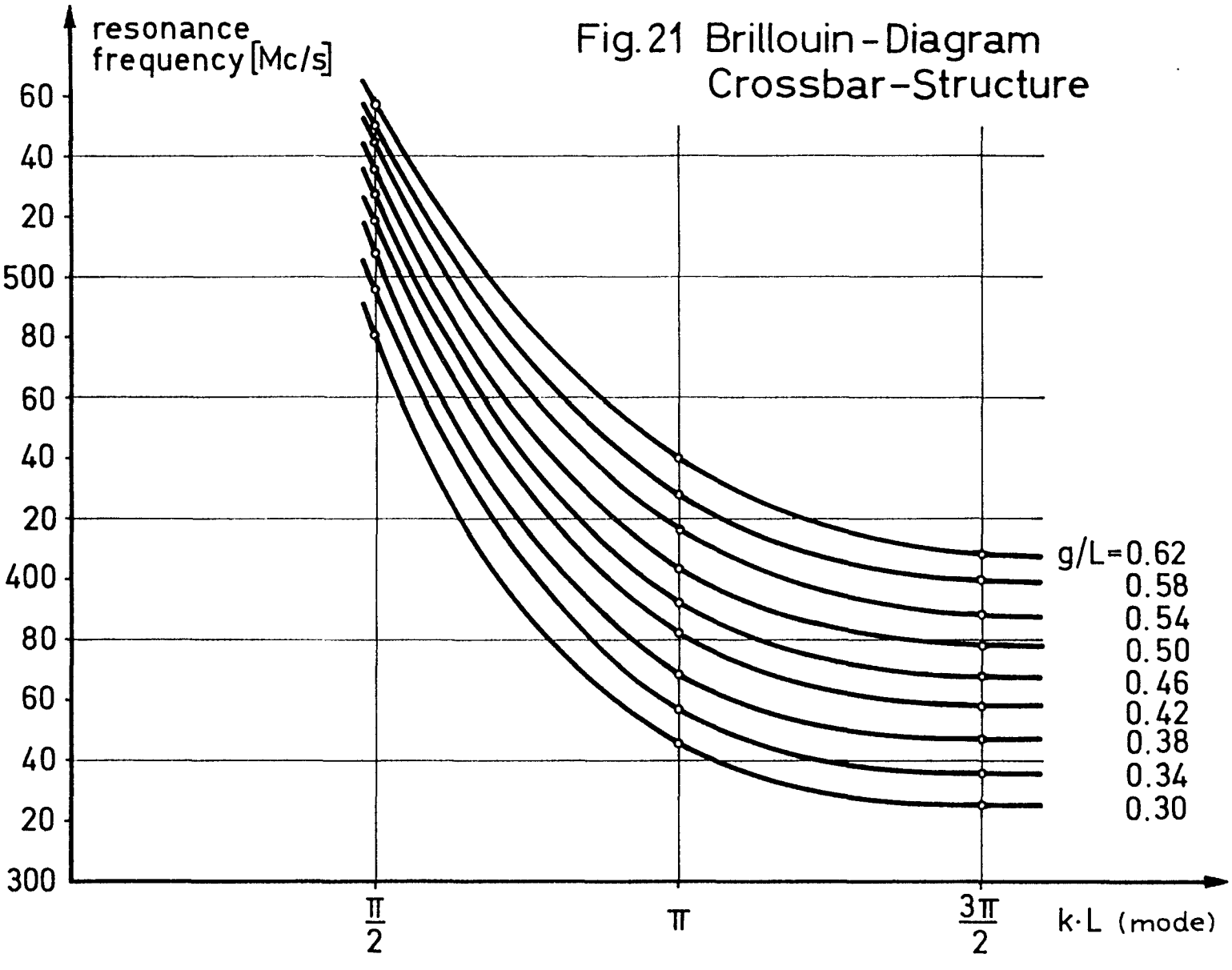

Fig. 21 Brillouin-Diagram
Crossbar-Structure

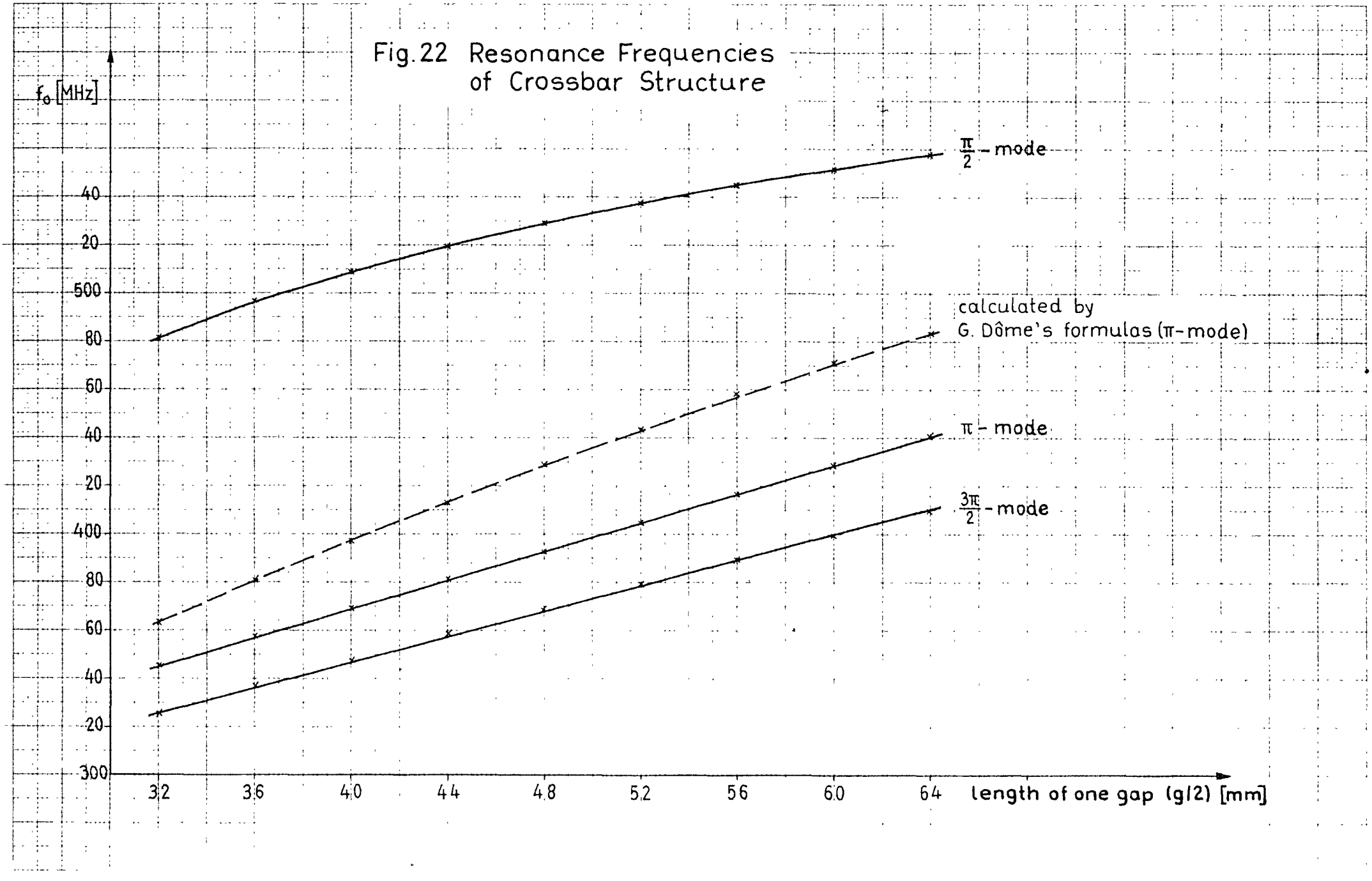
Fig. 22 Resonance Frequencies of Crossbar Structure
f_o [MHz]
40
20
500
80
60
40
20
400
80
60
40
20
300
3.2
3.6
4.0
4.4
4.8
5.2
5.6
6.0
6.4
length of one gap (g/2) [mm]
$\frac{\pi}{2}$ - mode
calculated by
G. Dôme's formulas (π-mode)
π - mode
$\frac{3\pi}{2}$ - mode

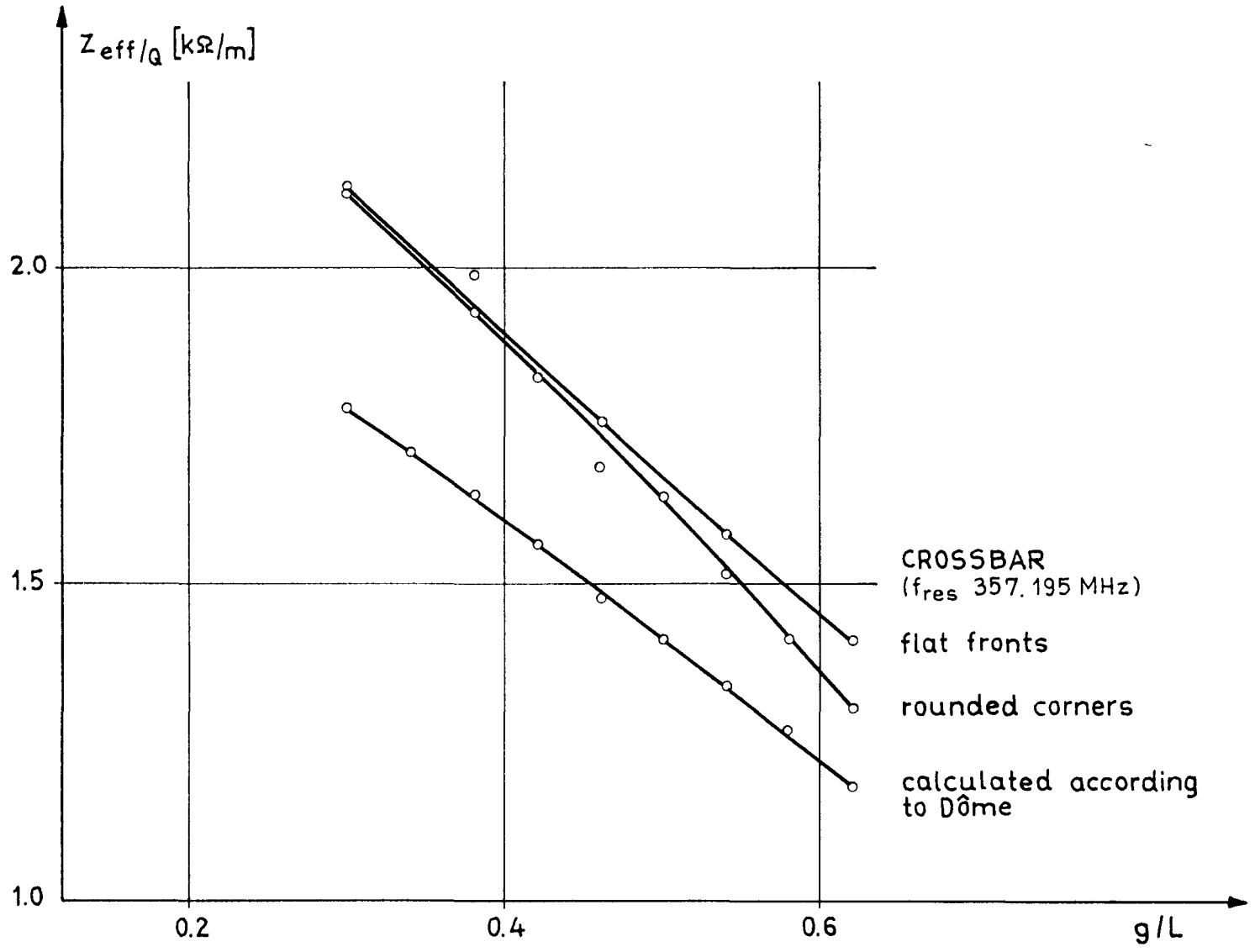
$Z_{eff/Q}$ [kΩ/m]
2.0
1.5
1.0
0.2
0.4
0.6
g/L
CROSSBAR
(f_{res} 357.195 MHz)
flat fronts
rounded corners
calculated according
to Dôme

Fig. 23

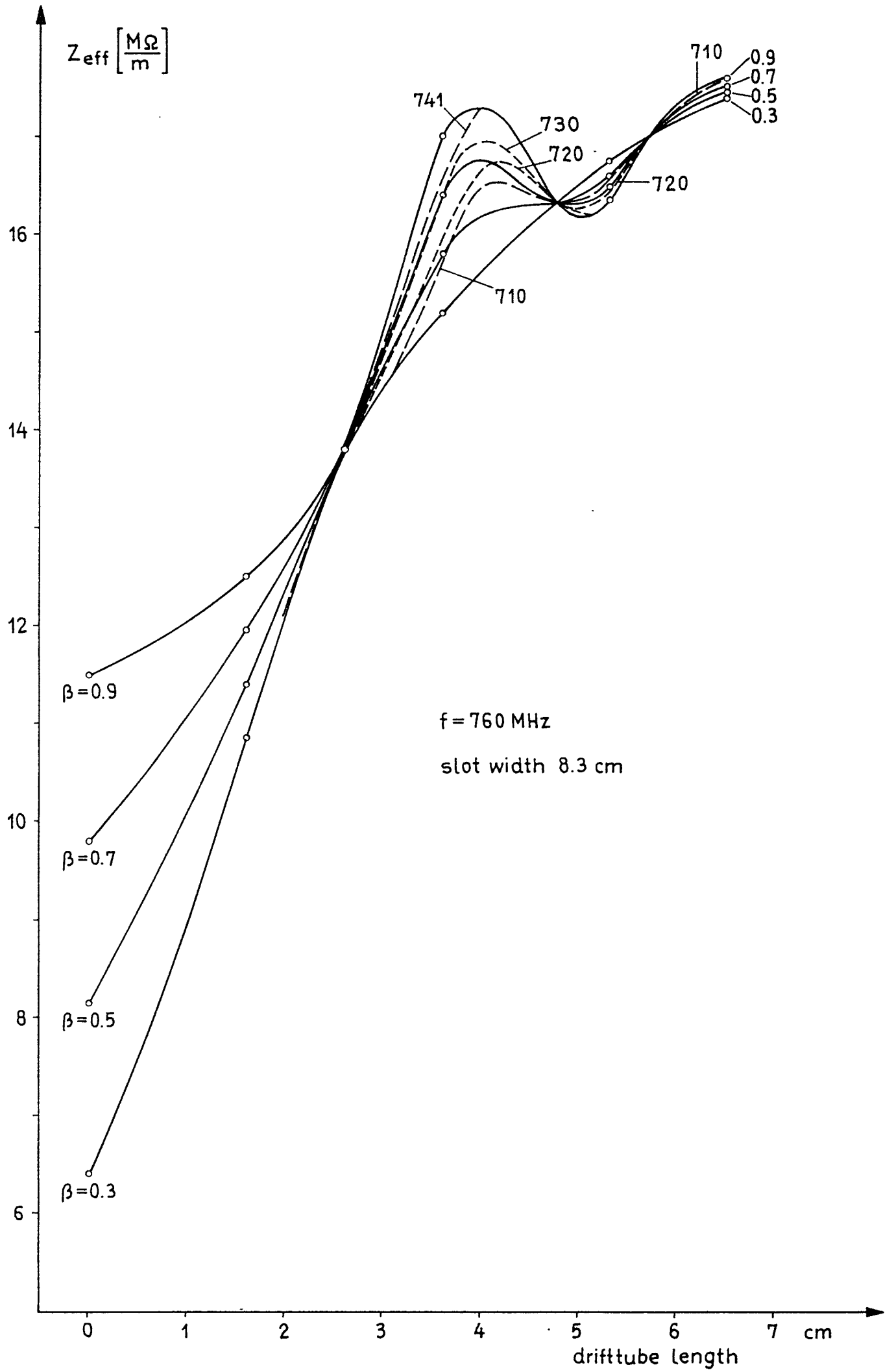
$Z_{eff}\left[\frac{M\Omega}{m}\right]$
741
730
720
710
720
710
0.9
0.7
0.5
0.3
16
14
12
10
8
6
β=0.9
β=0.7
β=0.5
β=0.3
f = 760 MHz
slot width 8.3 cm
0
1
2
3
4
5
6
7
cm
drifttube length

Fig. 24

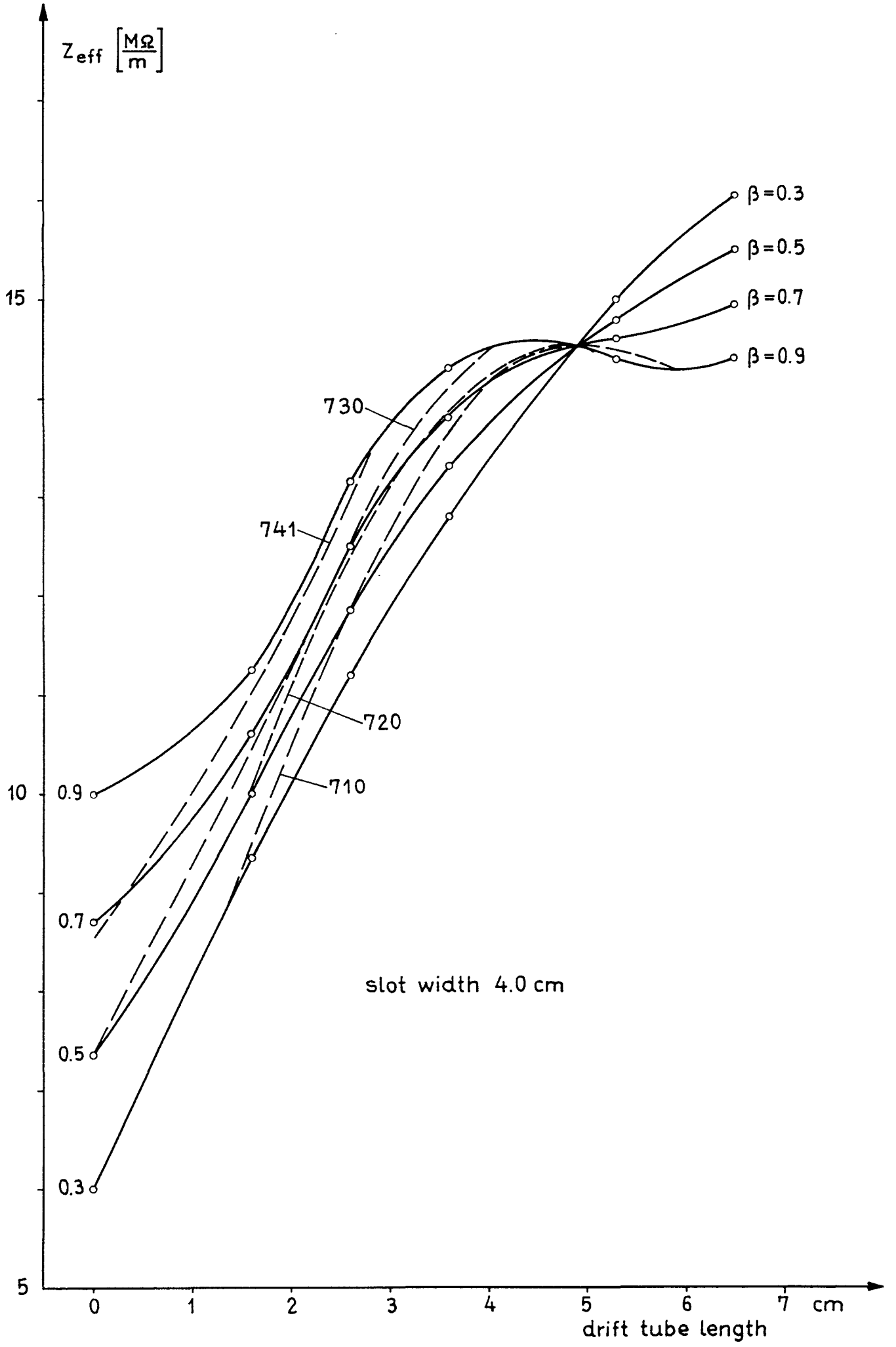
Z_{eff} $\left[\frac{M\Omega}{m}\right]$
15
10
5
β=0.3
β=0.5
β=0.7
β=0.9
730
741
720
710
0.9
0.7
0.5
0.3
slot width 4.0 cm
0
1
2
3
4
5
6
7 cm
drift tube length

Fig. 25

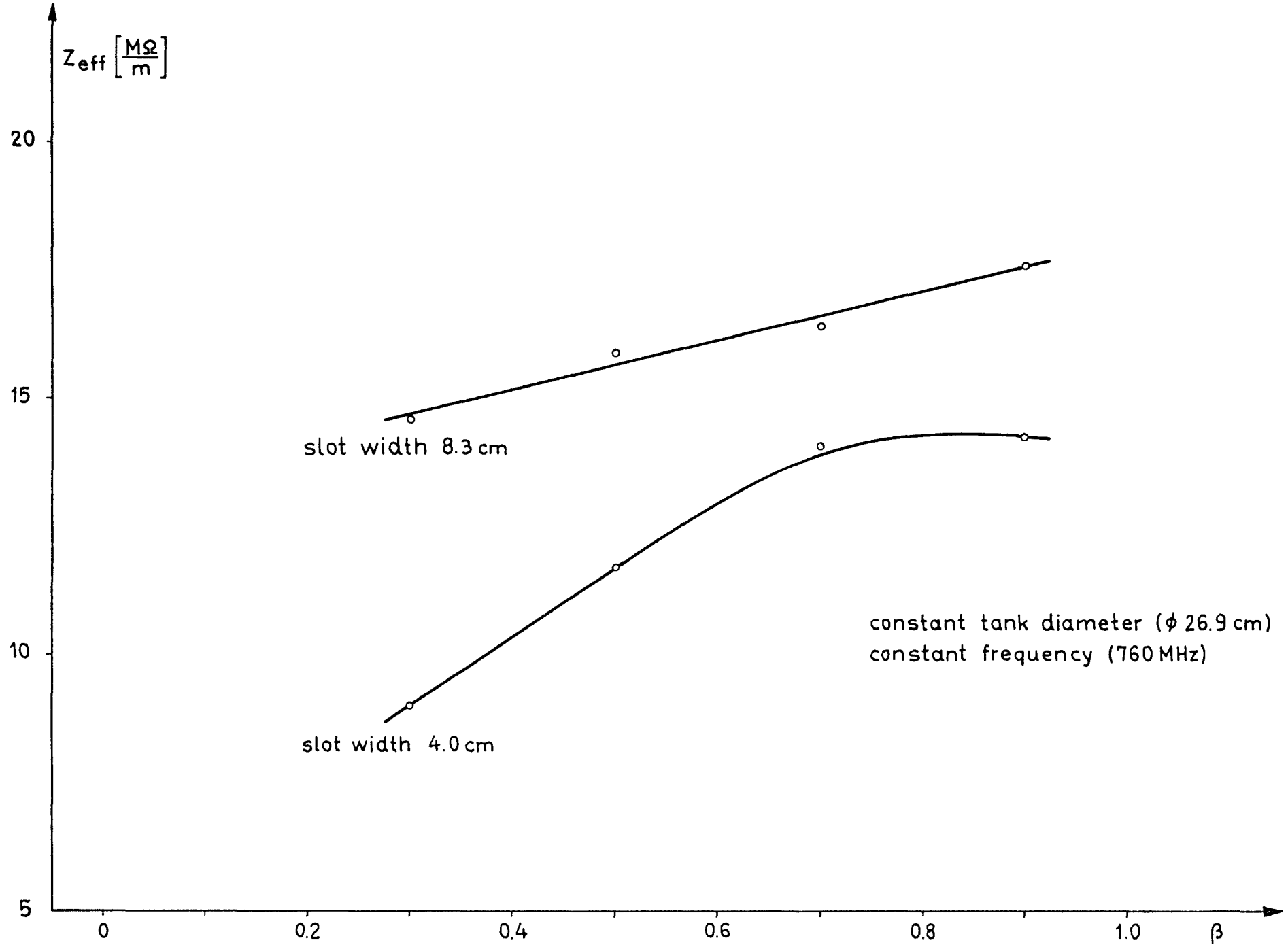
$Z_{eff}\left[\frac{M\Omega}{m}\right]$
20
15
10
5
0
0.2
0.4
0.6
0.8
1.0
β
slot width 8.3 cm
slot width 4.0 cm
constant tank diameter (ϕ 26.9 cm)
constant frequency (760 MHz)

Fig. 26